# Removal of Lead and Cadmium ions from Wastewater by Using Eco-friendly Nanocomposite

Abbas Mamdoh Abbas[a] Adel Sayed Orabi[a], Sayed Ahmed Eltohamy[b], Rasha Atef Shoman[b,*]

[a] Chemistry Department, Faculty of Science, Suez Canal University. Ismailia, 41522, Egypt.
[b] Environmental Research Department, Land, Water and Environment Institute, Agricultural Research Center(ARC), Ministry of Agriculture and Land Reclamation, 9-Cairo university street, Giza, 12112, Egypt.

Abstract
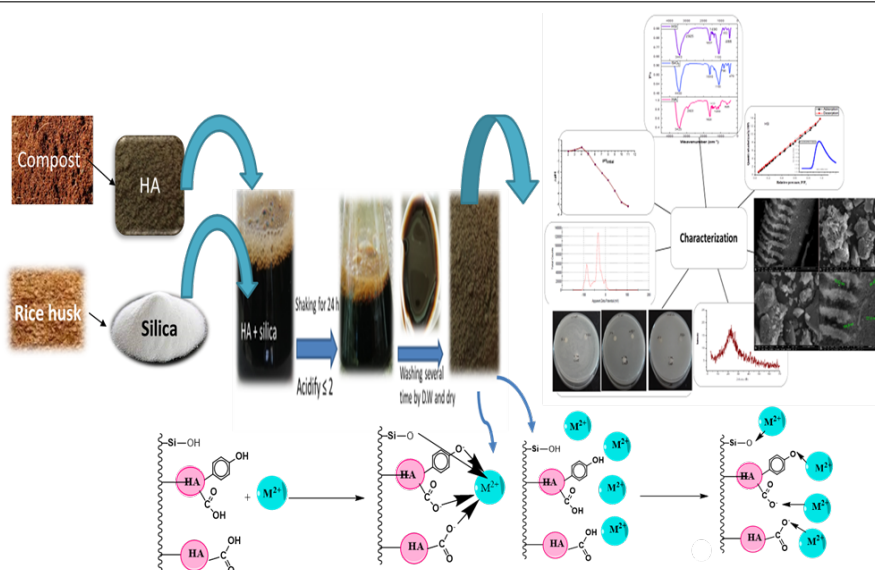
Eco-friendly nanocomposite (HS) was prepared from agriculture sources and characterized for remediation of wastewater from lead and cadmium ions. The nanocomposite was prepared from humic acid with silica (HS) which was prepared from compost and rice husk. The nanocomposite was characterized by FTIR, XRD, SEM, Zeta potential, BET and SEM-EDX. The removal of metal ions was studied using a variety of operating parameters, including pH, metal ion concentration, adsorbent dosage, and contact time. In both Pb^{2+} and Cd^{2+}, the best removal efficiency was found at pH 5.6 and 6. Pb^{2+} and Cd^{2+} had equilibrium times of 30 and 60 minutes, respectively. The adsorption process was exothermic and spontaneous in nature, according to thermodynamics. In terms of describing and evaluating the adsorption process, the Langmuir, Freundlich, and Temkin models are the most accurate, according to isotherm adsorption studies. Nanocomposite (HS) before and after adsorption was confirmed by EDX to involve lead and cadmium ions. The adsorption capacity of HS was 22.86 and 6.25 mg/g for Pb^{2+} and Cd^{2+}, respectively.

Keywords: Humic acid, Silica, Nanocomposite, Lead, Cadmium

1. Introduction

Pollution is the process of making land, water, air or other parts of the environment dirty and un-

safe or unsuitable to use [1]. This can be accomplished by dispersing pollutants into a natural setting. More than 200 million people around the world are affected by toxic pollution, according to Pure Earth, a non-profit environmental organization. Children in some of the world's most pol-

luted areas have lost 30 to 40 IQ points, and life expectancy may be as low as 45 years because of cancers and other diseases [2]. Chemicals, sewage, pesticides and fertilizers from agricultural runoff, or metals like lead or cadmium, are all examples of pollutants that can enter water sources [3]. Heavy metals can be removed from industrial wastewater by a variety of methods, precipitation, coagulation, complexation, activated carbon adsorption, solvent extraction, ion exchange, flotation, electrodeposition, foam flotation, cementation, and membrane operations. As a result, numerous novel approaches have been investigated to develop techniques for heavy metal adsorption that are both affordable and effective [4]. Adsorption is a fundamental process in the physicochemical treatment of municipal wastewaters, a treatment that can economically meet today's higher effluent standards and water reuse requirements. Adsorption is integral to a broad spectrum of physical, biological, and chemical processes and operations in the environmental field. Purification of gases by adsorption has played a major role in air pollution control, and adsorption of dissolved impurities from solution has been widely employed for water purification. Adsorption is now viewed as a superior method for wastewater treatment and water reclamation [5]. Nano-adsorbents got interest because of having nano-size, which can hold excellent rate of adsorption with short time. Furthermore, nano adsorbents that can used as a separation medium in water decontamination to eliminate the organic, inorganic-based pollutants [6]. Green synthesis provides advancement over chemical and physical method as it is cost effective, environment friendly, easily scaled up for large scale synthesis and in this method, there is no need to use high pressure, energy, temperature and toxic chemicals. This has motivated an upsurge in research on the synthetic routes that allows better control of shape and size for various nano technological applications [7].

The objective of this research was the preparation, and characterization of nanocomposite (HS) from humic acid and silica which were prepared from compost and rice husk ash respectively. Used this nanocomposite to remove some heavy met-als ions like (lead and cadmium ions). In the present study, we aimed to produce an economic, sustainable, good mechanical and chemical resistance, handleable, and regeneratable nanocomposite from agricultural residue as a sustainable adsorbent.

2. Experimental

2.1. Materials

Lead nitrate and cadmium nitrate were purchased from Sigma Aldrich as analytical grade reagents for this study. HCl, NaOH, KNO_3, $AgNO_3$ and disodium salt of ethylene diamine tetra acetic acid (Na_2EDTA) were purchased from Biochem. A compost sample and rice husk ash were purchased from Moshtohaor Agriculture station, Egypt.

2.2. Synthesis of sorbent

According to Sanchez–Monedero et al., humic substances were extracted [8]. Nanosilica has been prepared from rice husk as **Figures S1** and **S2**. Humic acid and silica composite (HS) with w/w ratio 1:1 was prepared as follows: 0.5 g humic acid and 0.5 g silica were dissolved in 15 ml of 0.5 N NaOH. The final solution was shaken for 24 hours. The composite (HS) was formed by acidifying the solution to a pH less than 2.0 using 2 N HCl. The composite has been collected by centrifuging for 15 minutes at 6000 rpm as shown in **Figure 1**.

2.3. Characterization Techniques:

An atomic absorption spectrophotometer, type AA-6800, Shimadzu, Japan, was used to determine the metal ions concentrations. To find out how porous the samples were and how much surface area they had, we used a Micromeritics ASAP 2000 volumetric adsorption device set to 77 K. The Zetasizer Ver.7.13 was used to analyze 1mg of composite in 10 ml of water (or additives solutions) for particle size distribution and Zeta potential (Malvern Panalytical). The BET equation was used to calculate surface area (SBET) for both samples (Brunauer-Emmett-Teller). Dubinin-Radushkevich (DR) and Barrett, Joyner, and Halenda (BJH) methods were used to calculate microporous and mesoporous volumes, respectively,
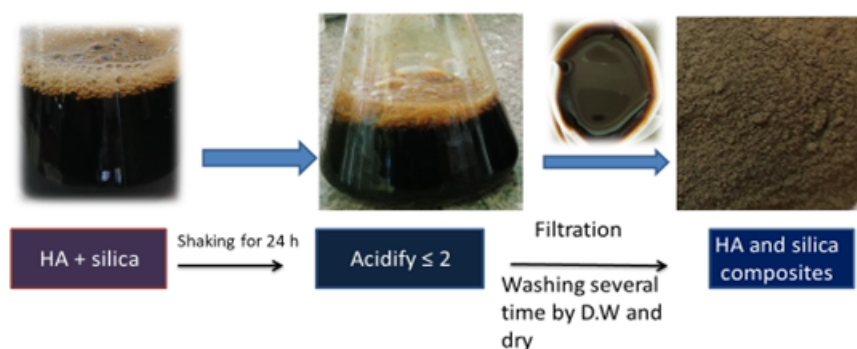
Figure 1: Schematic preparation andpurification of HS.

from the N_2 adsorption-desorption isotherm data (BJH). A scanning electron microscope (SEM) was used to examine the morphology of the adsorbent samples, and an energy dispersive spectrometer was connected to a power supply of 30 kV (EDX, Thermofisher). Silver lacquer and metallic gold or carbon-coated wafers were used to deposit samples. For Fourier-transform infrared spectroscopy in the 400-4000 cm^{-1} range, a Tensor 27 spectrophotometer (KBr disc) is used. Stuart Scientific muffling furnace (Vulcan A-550). After calibrating the pH meter (KnicK pH-meter model 761 Calimatic) using buffer solutions of pH 4, 7, and 10, the pH values were measured by the meter.

the pH_{PZC} for the nanocomposite was measured by the method of solid addition [9]. Here, 100 mg of the nanocomposite was added to 50 ml of 0.05 M KNO_3 in 50 ml steps. From 2 to 11, the pH values of these solutions have been increased by one (initial pHs,). Both 0.1 M HCl and 0.1 M NaOH solutions were used to bring the pH values back to normal. After that, for 48 hours, each flask was subjected to vigorous agitation in a shaker bath. After the suspensions had settled, the pH of each one was determined (final pHs). It was then compared to the initial pH values to see if there was a significant difference between them. The pH at which pH is zero determined to be the PZC [10]. the Antimicrobial Activity of HS nanocomposite had been tested by dissolving with sodium hydroxide and neutralized by dilute HCl. Results are presented as the diameter of the inhibitory zone measured in "mm", 0.06 mg of nanocomposite were added to discs according to the disc diffusion method, against the following indicator strains [11]: "Staph": Staphylococcus aureus (ATCC 25923), "E.coli": Escherichia coli (ATCC 25922) and "Candida": Candida albicans (ATCC 10231) with MacConkey Agar media, Mannitol Salt Agar, and Eosin Methylene Blue Staph, E.coli, and Candida isolates were tested for antimicrobial activity on agar prepared for this purpose. To ensure an even distribution of inoculums, the agar plate was stained with a bacterial-inoculated wipe and sterile tips were used to make the wells.

2.4. Solutions preparation

Pb^{2+} and Cd^{2+} ion stock solutions of 200 mg/L were prepared by dissolving 399.61 mg and 686.04 mg of lead nitrate and cadmium nitrate salts, respectively, in deionized water. 0.01 N $AgNO_3$ has been prepared as a standard solution for the determination of chloride ions by precipitation titration using potassium chromate as an indicator.

2.5. Batch experiments

2.5.1. The adsorption capacity

Adsorption was carried out in batch mode using 300 mg of adsorbent and a volume of 10 mL of adsorbate following the concentrations determined. Temperature, contact time, effect of dose, pH, and metal ion concentrations are all factors to consider. The recovered liquid phase was filtered after equilibrium time. Pb^{2+} and Cd^{2+} had pH of 4–6 and 4–8, respectively, and temperatures of 25–40 °C, while the initial metal ion concentrations varied between 50 and 250 mg/L in adsorption equilibrium experiments. Adsorption capacity q_e (mg/g) and removal efficiency q_e (mg/g) of

metal ions were calculated using these formulas (%) [12] :

$$Removal\ (\%) = \frac{(C_o - C_e)}{C_o}\ x100 \quad (1)$$

$$q_e = \frac{(C_0 - C_e) * V}{m}\ x\ 100 \quad (2)$$

The initial concentration of metal ions in the solution mixture was C_o, while the equilibrium concentration is C_e, and q_e is the equilibrium adsorption capacity (mg/g). V is the sample volume (L) and m is the mass of composite adsorbent used (g).

adsorbent isotherms are also crucial for describing the interactions between adsorbate molecules and adsorbent surface sites. For adsorption interpretation and prediction to be possible, equilibrium data must be correlated with a theoretical or empirical equation. In this study, Langmuir, Freundlich, and Temkin's isotherm equations are examined [13].

According to the Langmuir adsorption isotherm, inactive adsorption sites are unaffected by the presence or absence of nearby occupied adsorption sites. As a result of using the Langmuir isotherm equation to analyze lead uptake data [14]:

$$\frac{Ce}{Qe} = \frac{1}{Qm}Ce + \frac{1}{QmK_L} \quad (3)$$

The maximum monolayer coverage capacity, adsorption capacity of Q_e adsorbate, and the K_L Langmuir isotherm constant (L/mg) are all included in this equation.

The fundamental properties Langmuir isotherm can be expressed using an arbitrary constant separation factor R_L, as shown in the equation below [14]:

$$R_L = \frac{1}{(1 + K_L C_o)} \quad (4)$$

Where C_o is the adsorbate concentration (mg/L) at the highest adsorption point. There are four possible outcomes for R_L: linear, favorable, irreversible, and unfavorable for the isothermal shape when R_L exceeds 1, linear, and unfavorable for the isothermal shape when R_L is zero.

An empirical description of heterogeneous systems can obtained by using the Freundlich model. Here's how it's described mathematically [15]:

$$Q_e = K_f\ C_e^{1/n} \quad (5)$$

This equation has the following linear form:

$$\ln Q = \frac{1}{n}\ln C_e + \ln K_f \quad (6)$$

In this case, K_F and n were used as Freundlich constants. As the adsorption progresses, K_F measurements of the sorbent's adsorption capacity provide valuable information. One of the best indicators of adsorption preference is the exponent (1/n). If the adsorption 1/n is less than one, it indicates that the situation is typical. Until the number n is between 1 and 10, the absorption process is considered successful. There is empirical evidence that as temperature rises, the adsorption rate slows and more significant pressures are needed to completely saturated the surface [16]. For every molecule in the layer, Temkin's adsorption model predicts that the heat of adsorption decreases linearly as coverage grows [17]. Following is the equation that describes the model:

$$Q_e = B\ln C_e + b\ln A \quad (7)$$

(L/g) is the value of the Temkin isotherm constant, and R is the gas constant (8.314 J/mol K). B = RT/b, which is the Temkin constant related to the heat of sorption (J/mol) (K).

2.5.2. Adsorption Thermodynamics parameters

Thermodynamic equilibrium coefficients were measured at various concentrations and temperatures and then applied to the study of adsorption thermodynamic theory. Adsorption characteristics can be explained using thermodynamic quantities such as the Gibbs free energy change (ΔG^o), which can calculated using the following equation [18]:

$$\Delta G^o = -RT\ln K_d \quad (8)$$

where K_d is the equilibrium thermodynamic constant (L g^{-1}).

The adsorption enthalpy (ΔH^o) and entropy (ΔS^o) are divided by the temperature to obtain the Gibbs free energy (ΔG^o). The Van't Hoff plot can be used to determine ΔH^o and ΔS^o by applying this concept to the equation (8) and (9):

$$\ln K_d = -\Delta H^o/RT + \Delta S^o/R \quad (9)$$

2.5.3. Adsorption kinetics

The process of adsorption kinetics must be thoroughly studied to gain a better understanding of the mechanisms of adsorption. Studying adsorption rates for up to two hours, researchers compared the results of the experiment with theoretical models. Multiple pseudo-first- and second-order kinetic models were tested using data collected from experiments with varying contact times. Adsorption rate constant can be calculated with a pseudo-first-order equation (Lagergren equation) [19]:

$$\log(Q_e - Q_t) = \log Q_e - \frac{K_1}{2.303}t \qquad (10)$$

For equilibrium adsorption capacity, Q_e, Q_t, and K_1 represent the equilibrium rate constants (mg/g) of the adsorbent (mg/g). Pseudo-second order kinetics could benefit from an integrated second-order rate law [20]:

$$\frac{t}{Q1} = \frac{1}{Qe}t + \frac{1}{KQ_e^2} \qquad (11)$$

The pseudo-second-order rate constant is K_2 (g mg^{-1} min^{-1}).

The pseudo-second-order adsorption involves both chemical and physical processes. As the adsorbent and adsorbate share or exchange electrons, this could be a rate-limiting step in the adsorption process [20].

3. Results and discussion

3.1. Characterization

3.1.1. Infrared spectroscopy

FTIR of HS is shown in **Figure 2**. The main absorbance bands of HS were: strong band at 1638-1620 cm^{-1} due to olefinic and aromatic C=C, C=O stretching of COOH, ketones (trace), a shoulder at 1638-1510 cm^{-1} due to aromatic C=C, strong H-bond conjugated ketones quinone and amide, a band at 1510 cm^{-1} due to aromatic C=C and/or amide. Broad band between 3455 and 3417 cm^{-1} due to the frequency of H-bonding of O-H, N–H Stretching, CH_2 and CH_3 groups are deformed by C–H deformation and COO^- anti-symmetric stretching, while OH deformation

and C=O stretching of phenolic OH are responsible for a weaker band at 1384-1332 cm^{-1}. The COO^- symmetric stretching is responsible for the more prominent peak at 1422-1384 cm^{-1}, while the COO^- anti-symmetric stretching is responsible for the weaker band at 1384-1332 cm^{-1}, a sharp peak at 1104-1000 cm^{-1} due terminal group of the silanol group (Si-OH) a peak at 804 cm^{-1} due to aromatic ethers, possibly polysaccharides and Si-O of silicates and finally a band at 489 cm^{-1} due to Si-O-Si bend [21] [22].
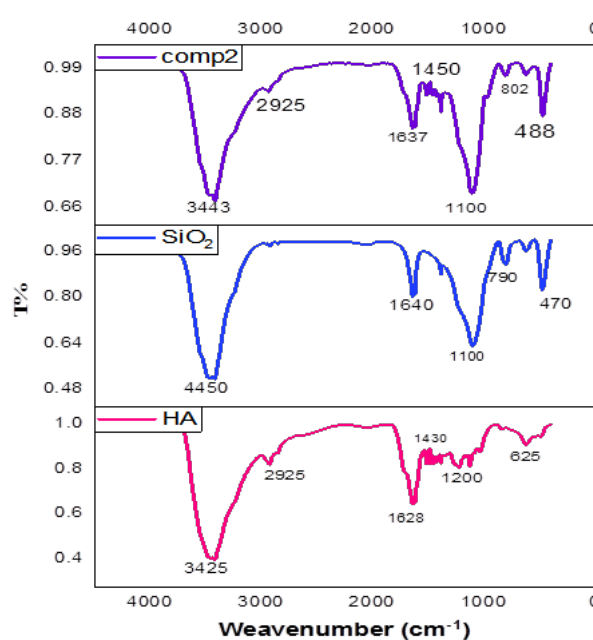

Figure 2: FT-IR spectrum of humic acid, silica and HS.

3.1.2. The X-ray powder diffraction (XRD pattern)

Figures (**S3, 3**) show the humic acid and silica XRD patterns, which show a diffuse pattern indicative of the amorphous phase and supported by XRD patterns. The nano SiO_2 and humic acid were synthesized from rice husk and compost respectively, successfully. The agglomeration of nanosilica particles and humic acid had a diameter of 10-30 nm. It has been found that the distribution of particle shapes is nearly uniform. The X-ray powder diffraction (XRD) pattern of HS has an average crystal size of 37.01nm using the Scherrer equation as shown in **Figure 3** [23].
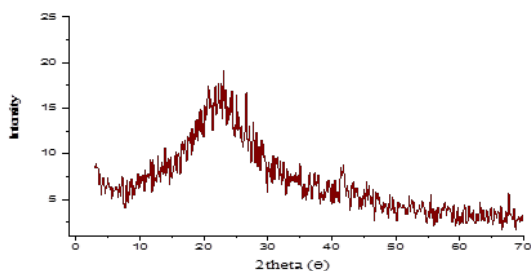
Figure 3: XRD of HS.

3.1.3. Zeta potential

The electro- kinetic potential of solid- liquid colloidal dispersion was measured and shown in **Table 1**, and represented in **Figure S4**. Zeta potential values are negative for nanocomposite. The value of potential for HS was -44.6 mV.

After dissolving acids from its surface, a negatively-charged layer will form on the particle. Instead, a neutral surface will become positively charged [24]. The strength of the acidic or basic surface groups, as well as the pH of the solution, affect the magnitude of the surface charge in both cases. In the case of negatively charged particles, surface ionization can be suppressed by lowering the pH [25]. In **Figure S5** HS pH_{PZC} was 4.5.

3.1.4. BET Analysis

Measurements of N_2 adsorption/desorption at 77.35 K^o were used to investigate the prepared nanocomposite's BET surface area and Barrette Joyner Halenda (BJH) pore size. Type III reversible isotherms, such as the N_2 adsorption-desorption isotherm of the nanocomposite, are convex along the x-axis. Moreover, it suggests an unrestricted multilayer formation process. These interactions are more powerful than those between molecules on both sides of an absorbent surface and the molecules they're holding onto [26] as shown in **Figure 4** and **Table S4**. This is the first steep part of the isotherm For the N_2 molecule's cross-sectional area, with a radius of 4.96e+001 nm, of the BET surface area for HS of 27.52 m^2/g. However, the average pore diameter is 1.53 nm and the total pore volume is 0.02 cm^3/g when measured at saturation pressure and expressed as liquid volume. Pore volume was 0.02 cm^3/g and Dv (d) was 1.77 nm for

BJH with a surface area of 12.38 m^2/g. Adsorption can benefit from the external surface area of 27.52 m^2/g that was calculated using the t-plot method.
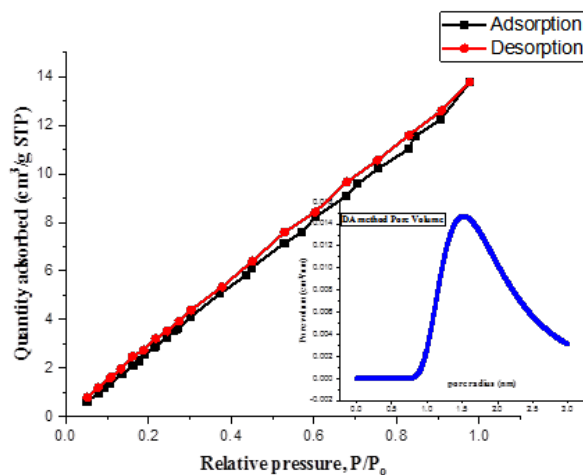
Figure 4: N_2 adsorption–desorption isotherms and corresponding pore size distribution curves(inset) of HS.

3.1.5. SEM analysis

SEM was employed to identify the surface texture, size morphology and porosity of nanoparticles of synthetic composite [27]. its average size was noted to be 84.48 nm. **Figure 5** showed the SEM of HS appeared with an irregular surface.
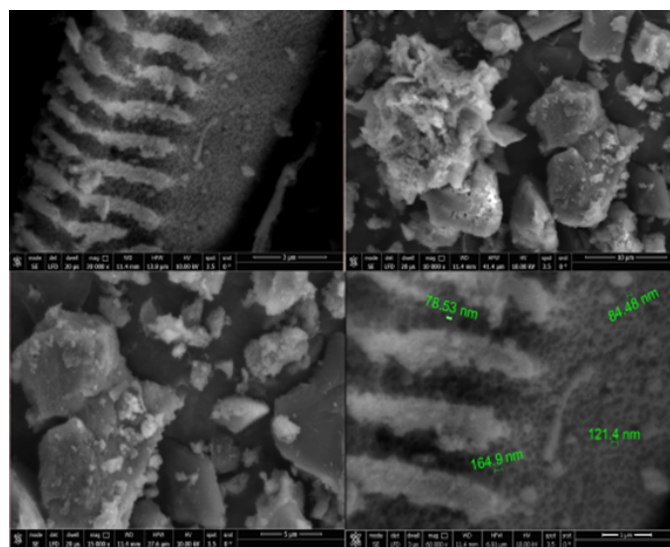

Figure 5: SEM of HS.

Table 1: Zeta potential analysis of nanocomposite (HS).

Mean(mV)	% Area	St. Dev.	Zeta potential (mV)	Zeta Deviation (mV)	Conductivity (mS/cm)
-31.2	61.2	9.58			
-86.4	23.5	7.54	-44.6	27.3	0.0167
-58.5	8.5	6.19			

3.1.6. Energy-dispersive X-ray spectroscopy (EDX)

The chemical compositions of prepared nanocomposite were determined by SEM-EDX analysis before and after Pb^{2+}, and Cd^{2+} adsorption, and shown in **Figure S6**. HS presents strong signals for C, O and Si which are the major components of humic acid and silica. The obtained results strongly confirm the retention of lead and cadmium ions. Which Pb^{2+} and Cd^{2+} peaks appeared, confirming the adsorption of these pollutants.

3.1.7. Studying the Antimicrobial Activity

The HS nanocomposite was added at a concentration of 0.06 mg/disc was added to one well and a positive control concentration was added to the third well. Following that, the plates were incubated for 16 hours at 37°C. All plates showed negative results for HS nanocomposite as shown in **Figure S7.**

3.2. The adsorption processes

The batch method was used for the adsorption process, as shown in **Table S5-S9** and **Figures (S8-S12)**. Removal of Pb^{2+} and Cd^{2+} increased by HS from 75.93% to 99.65% and 15.57% to 93.14%, respectively at weight (30-300 mg), and adsorption capacity decreased from 25.31 mg/g to 3.32 mg/g and 5.19 mg/g to 3.11 mg/g, respectively. Adsorption tests on HS were carried out in various pH solutions to investigate the impact of pH on the material's adsorption capacities. Aqueous solution pH affects the amount of Pb^{2+} and Cd^{2+} HS can take up. The adsorption capacity of Pb^{2+} and Cd^{2+} sorption increases from 3.31 mg/g to 3.33 mg/g and 1.55 mg/g to 3.17 mg/g, respectively. when the initial pH of the solution is from 4 to 6 and 4

to 8.16, respectively. The adsorption capacity of Pb^{2+} and Cd^{2+} increased from 8.29 mg/g to an undetected amount and 1.66 mg/g to 6.14 mg/g, respectively. when concentration increased from 50 to 250 mg/L. The adsorption is almost constant at whatever dye concentration if all of the sites are occupied. This indicates that the prepared composite surface has formed a monolayer. The adsorption reached equilibrium within 30 min (3.30 mg/g) for Pb^{2+} and 120 min (3.11 mg/g) for Cd^{2+}. The percent of the metal ions was removed gradually with time increases and reached its maximum level after 60 min (19.46 mg/g). The adsorption capacity of Pb^{2+} and Cd^{2+} decreased from 3.32 mg/g to 3.22 mg/g and 3.22 mg/g to 3.11 mg/g, respectively on HS was achieved at (25- 40°C).

3.3. Adsorption isotherm

The equilibrium data for the adsorption process are usually termed adsorption isotherms. When comparing the performance of different types of adsorbent under different operational conditions, it is important to know these factors. Classical adsorption isotherms are commonly used to model heavy metal adsorption. In this study, Langmuir, Freundlich, and Temkin isotherms models were used, and the values of various constants of the three models were calculated and represented in **Table 2**. Langmuir, Freundlich, and Temkin adsorption isotherms for Pb^{2+} and Cd^{2+} from aqueous solution have been linearized by using HS as adsorbent are presented in **Figures 6** and **7** (a, b, and c, respectively). All of the isotherm models were found to fit the data well in experiments.

In Langmuir's study, the correlation coefficients (R^2) give values 0.996 and 0.99 for Pb^{2+} and Cd^{2+} adsorption respectively. The Langmuir equation

is used to test the stability of the complex formed among metal ions and HS. In this study, the small K_L values 0.48 and 0.29 L.mg^{-1}, respectively, were obtained which indicate a strong binding of pollutants to HS surface. In this study, R_L value was found to be less than 1, which showed that the adsorption of Pb^{2+} and Cd^{2+} on HS was favorable and matched the Langmuir isotherm model well [28]. In this research, we found that: R_L value for Pb^{2+} and Cd^{2+} adsorption was found to be 8.26x10^{-3} and 14.0x10^{-3}, respectively, which are less than 1.

In the Freundlich study, Pb^{2+} and Cd^{2+} adsorption n values were found to be 0.76 and 4.66, respectively. Adsorption isotherms are concave in the case of Cd^{2+} and Pb^{2+}, and 1/n values less than 1 indicate weaker free energies and favorable adsorption. However, in the case of Pb^{2+}, 1/n values greater than 1 indicate stronger free energies and less favorable adsorption. The correlation coefficients (R^2) for Pb^{2+} and Cd^{2+} adsorption give values of 0.999 and 0.9998, respectively which are the highest value as compared to the Temkin model. It was observed that the Freundlich isotherm gives a good fit model than the Temkin isotherm model. Thus, the adsorption for Pb^{2+} and Cd^{2+} adsorption onto HS follows a multilayer adsorption process.

In the Temkin study, it was observed that the heat of sorption is equal to 1.42 and 2.56 KJmol^{-1} for Pb^{2+} and Cd^{2+} respectively.

3.4. Adsorption Thermodynamics

The slope and y-intercept of a linear plot for lnK$_d$ versus 1/T were used to calculate ΔH° and ΔS°. According to the findings, enthalpy of HS with Pb^{2+} and Cd^{2+} adsorption ΔH° was -13.87 and -42.96 kJ mol^{-1} and ΔS° were -390 and 40 kJ mol^{-1}K^{-1}, respectively. However, even though these values of enthalpy ΔH^o are not very high, they can be explained by the fact that the metal ions and HS have a considerable amount of interaction during the exchange process. as shown in **Figure S9** and illustrated in **Table 3**.

The following equation was used to calculate the ΔG^o at various temperatures:

$$\Delta G^o = \Delta H^o + T\Delta S^o \qquad (12)$$

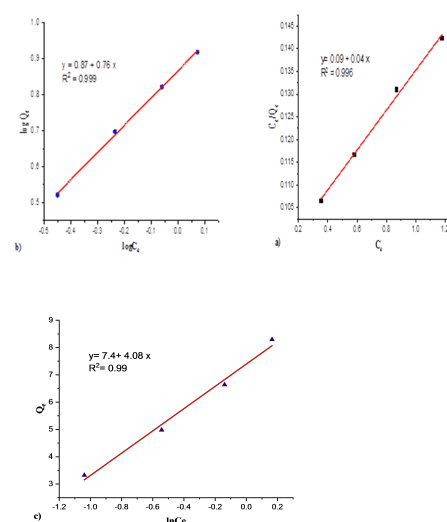Negative values of ΔG^o point that adsorption is spontaneous at these temperatures. The negative

Figure 6: Adsorptionisotherms of Pb^{2+} on HS using: a) Langmuir model b) Freundlich model c) Temkin model. (Temp.= 25°C,weight =300 mg., pH= 5.6, time=120 min, sol. volume= 10 mL).
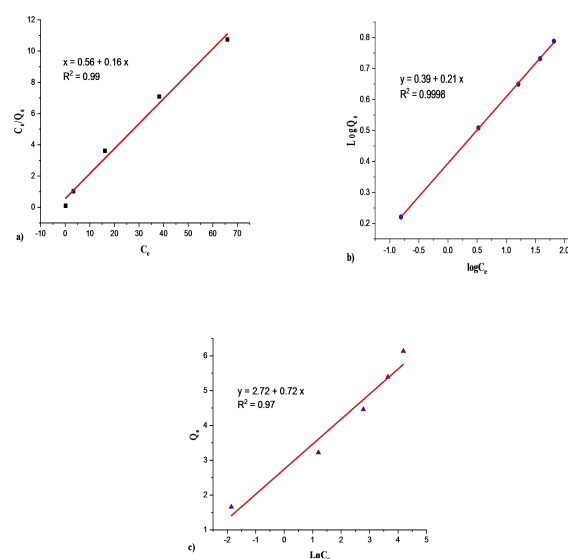
Figure 7: Adsorption isotherms of Cd^{2+} on HS using: a) Langmiur model b)Freundlich model c) Temkin model (Temp.= 25°C, time= 120 min., pH= 6, adsorbent dose= 300 mg,sol. volume= 10 mL).

ΔH° denotes that this adsorption is an exothermic process, declaring that this adsorption is promoted at low temperatures. A variety of materials, modified biomass ash and nanoparticles modified with Schiff bases as well as manganese oxide minerals

Table 2: Parameters and correlation coefficient of Langmuir, Freundlich and Temkin isotherm model for adsorption ofPb^{2+} and Cd^{2+} onto HS.

isotherm model s	Parameters and correlation coefficient	Isotherm model for adsorption of Pb^{2+}	Isotherm model for adsorption of Cd^{2+}
Langmuir isotherm model parameters	q$_m$ (mg/g)	22.80	6.25
	K$_L$ (L/mg)	0.48	0.29
	R$_L$X 10^{-3}	8.26	14.0
	R^2	0.996	0.99
Freundlich isotherm model parameters	1/n	1.32	0.22
	n	0.76	4.66
	K$_F$= (mg/g (L/mg)1/n)	7.38	2.48
	R^2	0.999	0.9998
Temkin isotherm model parameters	A (L/g)	7.40	2.74
	b (kJ/mol)	1.42	2.56
	B	4.08	0.72
	R^2	0.99	0.97

were found to Pb^{2+} and Cd^{2+} from water [29].

3.5. Adsorption kinetics

The linearity of the pseudo-second-order model is superior to that of the pseudo-first-order model, as shown in **Table 4** and **Figures** (**S16, S17**). The q$_{e,cal}$ data generated by the pseudo-second-order model matched the experimental results, indicating the suitability of this model for simulations of real-world data. Because of this, the metal ion adsorption kinetics on HS nanocomposite can be accurately described by the pseudo-second-order model. The second-order model suggests that the boundary layer resistance was not an impediment to progress. An intraparticle mass transport mechanism located within the sorbent governed the adsorption rate in this case. It appears that diffusion occurs in the initial stage, following the experimental findings from the model's linearized regression Morris and Weber (about 15 min). For this model, the diffusion process appears to be going fairly well in the early stages [30].

3.6. Adsorption mechanism

On the HS surface, we found that the ion exchange or complexation between metal ions, carboxylic and/or polyphenolic groups may play an important role in adsorption. **Figure 8** depicts two possible representations of the Pb^{2+}/HS and

Cd^{2+}/HS reactions. Adsorption mechanisms based on similar reaction pathways have been proposed for a variety of metal ions on HS adsorbents. [31].

The Langmuir isotherm adsorption capacity parameter, q$_{max}$, is frequently used to assess adsorbent performance. **Table 5** summarises the q$_{max}$ values of several adsorbents reported in the literature. HS composite exhibits good metal ions adsorption capacity when compared to prior studies, according to the findings of this investigation. HS's employment in removing metal ions is highly promising because of its low cost, widespread availability, and intriguing adsorption potential.
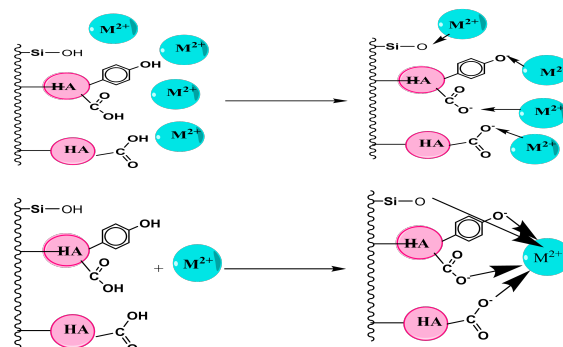

Figure 8: Adsorptionmechanism by HS adsorbent. Ligand site of nanocomposite shown are carboxylicand phenolic.

Table 3: The thermodynamic parameters of Pb^{2+} and Cd^{2+} adsorption on HS.

The thermodynamic parameters of Pb^{2+}						The thermodynamic parameters of Cd^{2+}					
ΔH^o (kJ/mol)	ΔS^o (J/mol.K)	ΔG^o (kJ/mol)				ΔH^o (kJ/mol)	ΔS^o (J/mol.K)	ΔG^o (kJ/mol)			
		298	303	308	313			298	303	308	313
13.87	-390	-22.66	-23.89	-18.81	-17.87	-42.96	40	-17.04	-17.17	-16.35	-15.93

Table 4: Parameters of pesudofirst-order andpseudosecond-order for adsorption of Pb^{2+} and Cd^{2+} onto HS nanocomposite.

Adsorbent/adsorbate		HS/Pb^{2+}	HS/Cd^{2+}
Pseudofirst-order kinetic parameters	Q_e cal	1.54	1.26
	K_1	1.54	0.03
	R^2	0.74	0.87
Pseudosecond-order kinetic parameters	Q_e cal	20.11	3.3
	K_2	0.06	0.04
	R^2	0.99989	0.99888

Table 5: Monolayeradsorption capacities (q_{max} in mg/g) in the literature foradsorption of Pb^{2+} and Cd^{2+} on various adsorbents.

Adsorbent	qmax (mg/g)		References
	Cd^{2+}	Pb^{2+}	
Nanocomposite humic acid and silica (HS)	22.80	6.25	This study
Humic acid	22.70	-	[32]
Activated carbon (Merck)	21.50	-	[33]
Coir	19.87	-	[34]
Carbon nanotubes	17.44	-	[35]
Jute	17.18	-	[34]
Groundnut shells	12.21	-	[34]
Goethite	11.04	-	[32]
Montmorillonite	10.40	-	[32]
Saw dust	3.19	-	[36]
Waste tea leaves	2.096	-	[37]
Olive stone carbon	-	5.91	[38]
Almond-shell carbon	-	2.7	[39]

3.7. Remediation of wastewater samples from metals ions

Six wastewater samples, from six sites in two locations in Ismailia, were collected to determine the sorption performance of the synthesized four composite adsorbents. The results were shown in **Table S10 and S11**. At pH 5.5, with 0.5 mg/L nanocomposite, 2 h shaking time and room temperature, the remediation rates of selected heavy metals were studied. The remediation rates of HS nanocomposite for Pb^{2+} at Cd^{2+} more than 99.99 % in the presence of coexisting ions (Na^+, K^+, Mg^{2+} and Ca^{2+}). These experiments demonstrated that nanocomposite prepared using specific methods had a significant impact on environmental cleanup and wastewater treatment.

References

[1] A. G. A, I, Relationship between environment and sustainable economic development: A theoretical approach to environmental problems, J. of Asian Social Science 3 (3) (2013) 741–761.

[2] P. M. Senge, B. Smith, N. Kruschwitz, J. Laur, S. Schley, THE NECESSARY REVOLUTION: HOW INDIVIDUALS AND ORGANIZATIONS ARE WORKING TOGETHER TO CREATE A SUSTAINABLE WORLD, Strategic Direction, 2008. doi:doi.org/10.1108/sd.2009.05625hae.001.

[3] P. Chowdhary, R. N. Bharagava, S. Mishra, N. Khan, Role of Industries in Water Scarcity and Its Adverse Effects on Environment and Human Health, Environ. Concerns Sustain. Dev (2020) 235–256doi:doi.org/10.1007/978-981-13-5889-0_12.

[4] S. Mishra, Heavy Metal Contamination: An Alarming Threat to Environment and Human Health, Environ. Biotechnol. Sustain. Futur (2019) 103–125.

[5] Y. C. Wong, M. S. R. Senan, N. A. Atiqah, Removal of methylene blue and malachite green dye using different form of coconut fibre as absorbent, Journal of Basic & Applied Sciences 9 (2013) 172–177. doi:10.6000/1927-5129.2013.09.23.

[6] R. B. Onyancha, U. O. Aigbe, K. E. Ukhurebor, W. B. Muchiri, Facile synthesis and applications of carbon nanotubes in heavy-metal remediation and biomedical fields: A comprehensive review, Journal of Molecular Structure 1238 (2021) 130462. doi:doi.org/10.1016/j.molstruc.2021.130462.

[7] M. Pattanayak, P. L. N, Green synthesis and characterization of zero valent iron nanoparticles from the leaf extract of Azadirachta indica (Neem)," academia.edu, Nano Science & Technology, 13 (2) (2012) 16–22.

[8] M. A. Sánchez-Monedero, J. Cegarra, D. García, A. Roig, Chemical and structural evolution of humic acids during organic waste composting, Biodegradation 13 (6) (2002) 361–371.

[9] D. Kołodyńska, J. Bąk, M. Kozioll, L. V. Pylypchuk, Investigations of Heavy Metal Ion Sorption Using Nanocomposites of Iron-Modified Biochar, Nanoscale Res. Lett 12 (2017) 433–444.

[10] T. Mahmood, M. T. Saddique, P. Westerhof, S. Mustafa, A. Alum, Comparison of different methods for the point of zero charge determination of NiO, Comparison of different methods for the point of zero charge determination of NiO 50 (7) (2011) 10017–10023. doi:doi.org/10.1021/ie200271d.

[11] S. C. Beristain-Bauza, E. Mani-López, E. Palou, A. Lopez, Antimicrobial activity and physical properties of protein films added with cell-free supernatant of Lactobacillus rhamnosus, Control, and undefined 2016 62 (2016) 44–51. doi:doi.org/10.1016/j.foodcont.2015.10.007.

[12] J. Goel, K. Kadirvelu, C. Rajagopal, Pb(II) and Hg(II) ions from aqueous solution using cocnut shell-based activated carbon, Adsorption Science and Technology 22 (3) (2004) 257–273.

[13] A. Bonilla-Petriciolet, D. Mendoza-Castillo, Adsorption processes for water treatment and purification(2017).

[14] H. Swenson, N. P. Stadie, Langmuir's Theory of Adsorption: A Centennial Review, American Chemical Society 35 (16) (2019) 5409–5426.

[15] R. Saadi, Z. Saadi, R. Fazaeli, N. E, F. K (2015).

[16] J. P. Stratford, Surface properties and adsorption capacity of biomass derived pyrolytic carbons (2012).

[17] P. S. Kumar, S. Ramalingam, C. Senthamarai, M. Niranjanaa, P. Vijayalakshmi, S. Sivanesan, Adsorption of dye from aqueous solution by cashew nut shell: studies on equilibrium isotherm, kinetics and thermodynamics of interactions 261 (1-2) (2010) 52–60. doi:doi.org/10.1016/j.desal.2010.05.032.

[18] X. jiangHu, J. songWang, Y. guoLiu, Adsorption of chromium (VI) by ethylenediamine-modified cross-linked magnetic chitosan resin: isotherms, kinetics and thermodynamics 185 (1) (2011) 306–314. doi:doi.org/10.1016/j.jhazmat.2010.09.034, [link]. URL https://www.sciencedirect.com/science/article/pii/S0304389410011933

[19] D. G. Strawn, A. M. Scheidegger, D. L. Sparks, Kinetics and mechanisms of Pb(II) sorption and desorption at the aluminum oxide - Water interface, Environ. Sci. Technol 32 (17) (1998) 2596–2601.

[20] L. Seifi, A. Torabian, H. Kazemian, G. N. Bidhendi, A. A. Azimi, F. Farhadi, S. Nazmara, Kinetic study of BTEX removal using granulated surfactant-modified natural zeolites nanoparticles, Water. Air. Soil Pollut 219 (1-4) (2011) 443–457. doi:DOI 10.1007/s11270-010-0719-z.

[21] T. Carballo, M. V. Gil, X. Gómez, F. González-Andrés, A. Morán, Characterization of different compost extracts using Fourier-transform infrared spectroscopy (FTIR) and thermal analysis, Biodegradation 19 (6) (2008) 815–830.

[22] B. A. Morrow, A. J. McFarlan, Surface vibrational modes of silanol groups on silica, J. of Physical Chemistry 96 (3) (1992) 1395–1400. doi:doi.org/10.1021/j100182a068.

[23] F. T. L. Muniz, M. A. R. Miranda, C. M. Santos, J. M. Sasaki, The Scherrer equation and the dynamical theory of X-ray diffraction, Acta Crystallogr. Sect. A Found. Adv 72 (3) (2016) 385–390.

[24] D. V. McCalley, Study of retention and peak shape in hydrophilic interaction chromatography over a wide pH range, Journal of Chromatography A 1411 (2015) 41–49. doi:doi.org/10.1016/j.chroma.2015.07.092.

[25] A. M. Badawy, T. P. Luxton, R. G. Silva, K. G. Scheckel, M. T. Suidan, T. M. Tolaymat, Impact of environmental conditions (pH, ionic strength, and electrolyte type) on the surface charge and aggregation of silver nanoparticles suspensions, Environ. Sci. Technol 44 (4) (2010) 1260–1266.

[26] M. Kruk, M. Jaroniec, Gas adsorption characterization of ordered organic-inorganic nanocomposite materials, Chem. Mater 13 (10) (2001) 3169–3183.

[27] K. Jayaramulu, F. Geyer, M. Petr, R. Zboril, D. Vollmer, R. A. Fischer, Shape Controlled Hierarchical Porous Hy-

drophobic/Oleophilic Metal-Organic Nanofibrous Gel Composites for Oil Adsorption, Adv. Mater 29 (12) (2017). doi:https://doi.org/10.1002/adma.201605307.

[28] M. Naushad, Z. A. Alothman, M. R. Awual, M. M. Alam, G. E. Eldesoky, Adsorption kinetics, isotherms, and thermodynamic studies for the adsorption of Pb2+ and Hg2+ metal ions from aqueous medium using Ti (IV) iodovanadate cation , Springer 21 (8) (2015) 2237–2245.

[29] A. Ramdani, A. Kadeche, M. Adjdir, Z. T. .-W. Practice, . . . , Lead and cadmium removal by adsorption process using hydroxyapatite porous materials , Water Practice & Technology 15 (1) (2020) 130–141. doi:doi.org/10.2166/wpt.2020.003.
URL https://iwaponline.com/wpt/article-abstract/15/1/130/71825

[30] R. Yu, X. Yu, B. Xue, J. Liao, W. Zhu, S. Tian, Adsorption of chlortetracycline from aquaculture wastewater using modified zeolites, J. Environ. Sci. Heal. - Part A Toxic/Hazardous Subst. Environ. Eng 55 (5) (2020) 573–584.

[31] G. K. Sarma, S. S. Gupta, K. G. Bhattacharyya, Nanomaterials as versatile adsorbents for heavy metal ions in water: a review, Environ. Sci. Pollut. Res 26 (7) (2019) 6245–6278.

[32] Z. Wu, Z. Gu, X. Wang, L. Evans, H. G, . E, Effects of organic acids on adsorption of lead onto montmorillonite, goethite and humic acid, Environmental Pollution 121 (3) (2003) 469–475. doi:doi.org/10.1016/S0269-7491(02)00272-5.
URL https://www.sciencedirect.com/science/article/pii/S0269749102002725

[33] J. Rivera-Utrilla, I. Bautista-Toledo, M. A. Ferro-García, C. Moreno-Castilla, Activated carbon surface modifications by adsorption of bacteria and their effect on aqueous lead adsorption, Wiley Online Libr 76 (12) (2001) 1209–1215.

[34] S. R. Shukla, R. S. P, Removal of Pb (II) from solution using cellulose-containing materials, Wiley Online Libr 80 (2) (2005) 176–183.

[35] Y. H. Li, S. Wang, J. Wei, X. Zhang, C. Xu, Z. Luan, D. Wu, B. Wei, Lead adsorption on carbon nanotubes, Chemical Physics Letters 357 (3-4) (2002) 263–266. doi:doi.org/10.1016/S0009-2614(02)00502-X.

[36] B. Yu, Y. Zhang, A. Shukla, S. S. S, J (2001). [link].
URL https://www.sciencedirect.com/science/article/pii/S0304389401001984

[37] S. S. Ahluwalia, D. G, . E, Removal of heavy metals by waste tea leaves from aqueous solution, life Sciences, and undefined 5 (2005) 158–162.

[38] M. A. Ferro-Garcia, J. Rivera-Utrilla, J. R. Gordillo, B. Toledo, Adsorption of zinc, cadmium, and copper on activated carbons obtained from agricultural by-products, Carbon 26 (3) (1988) 363–373. doi:Doi.org/10.1016/0008-6223(88)90228-X.

[39] C. A. Toles, W. E. Marshall, Copper ion removal by almond shell carbons and commercial carbons: Batch and column studies, Sep. Sci. Technol 37 (10) (2002) 2369–2383.